



M Ű E G Y E T E M 1 7 8 2

BUDAPEST UNIVERSITY OF TECHNOLOGY AND ECONOMICS  
FACULTY OF CIVIL ENGINEERING

PÁL VÁSÁRHELYI DOCTORAL SCHOOL OF CIVIL ENGINEERING AND EARTH SCIENCES

# **Laboratory testing and numerical modelling of water transport in concrete**

*New scientific results of the PhD dissertation*

**Miklós Pap**

Civil Engineer

Scientific supervisor:

**András Mahler, PhD**

Associate Professor

Budapest, 2025

# **1 INTRODUCTION**

Over the past decades, investigations conducted on unsaturated soils have demonstrated that even a slight reduction in the degree of saturation can significantly decrease the soil's hydraulic conductivity (Fredlund, et al., 2012). Similar trends have been observed in other porous materials, such as geotextiles and asphalts (Park & Fleming, 2006; Renken, et al., 2016; Törzs, et al., 2019; Fleming, et al., 2023). Furthermore, numerous publications confirm that changes in the water content of porous media, including rocks and soils, have a considerable impact on their mechanical properties (Pezowicz & Choma-Moryl, 2015; Vásárhelyi & Davarpanah, 2018; Zhang, et al., 2023; Ma, et al., 2023). Previous experimental studies conducted on concrete specimens suggest that a similar relationship can be observed for concrete in terms of water permeability. Consequently, it can be hypothesized that soil mechanics models developed for unsaturated media may also be extended to describe water flow in other porous materials, such as concrete (Leech, et al., 2003; Major, et al., 2010; Major & Wittmann, 2011; Vilasboas, et al., 2016; Pap, et al., 2018; Liu, et al., 2020).

The relevance of this topic is underscored by the fact that the presence of water during geotechnical construction works is almost inevitable. In the case of diaphragm wall excavations, it is of particular importance to create a concrete structure with the highest possible watertightness. However, the production of fully impermeable concrete is practically unattainable. For construction pits that remain open for an extended period, knowledge of the permeability function becomes especially critical, as it enables the estimation of the volume of water that may seep through the structure and provides evidence as to whether water will infiltrate within a specified timeframe.

In the case of waste disposal facilities – especially those designed for the storage of hazardous or radioactive waste – the understanding of saturation-dependent permeability values is even more crucial (Carme & Saaltink, 2016). For such structures, a fundamental requirement is to prevent water from entering or exiting the system. The permeability function enables the numerical modelling of water movement within the concrete used in storage facilities.

Beyond these aspects, analyzing water transport within concrete can also contribute to studies of concrete and reinforcement steel corrosion, as well as to the long-term evaluation of corrosion processes. By considering the variations in permeability and saturation, it is possible to more accurately estimate the onset and rate of corrosion, which is of fundamental importance for the design of durable concrete structures.

## 2 OBJECTIVES OF THE DISSERTATION

During my undergraduate and master's studies, through diploma theses and Scientific Students' Association research, I investigated laboratory methods for characterizing water transport in concrete and explored the potential of finite element modeling for simulating water seepage. The promising results underscored the need for more advanced and systematic investigations.

Considering the above, the primary aim of this doctoral research is to provide a comprehensive investigation of experimental and numerical approaches for analyzing water transport in concrete.

Building on previous work, the main research objectives are as follows:

- a) Laboratory measurement of drying and wetting water retention curves for concretes.
- b) Investigation of the hysteresis between the drying and wetting branches.
- c) Analysis of laboratory boundary conditions, sample type and size effects, as well as the uncertainties associated with water content measurements.
- d) Calculation of the permeability function over the full suction range based on the measured water retention curves.
- e) Measurement of the saturated hydraulic conductivity of concretes.
- f) Validation of the experimental results by means of finite element simulation of the standardized concrete watertightness test.
- g) Investigation of the water retention characteristics of concrete through pore structure analysis.
- h) Analysis of the results of the standardized watertightness test in relation to the concrete's porosity and hydraulic properties.
- i) Formulation of recommendations regarding the selection of models, parameters, and boundary conditions applicable for the calculation of water transport in concrete.

## 3 MATERIALS AND METHODS

The primary objective of the laboratory investigations was to generate the necessary data for analyzing water transport in concrete and to determine the input parameters essential for numerical modelling. As the first step of this chapter, I provide a description of the investigated concrete mixtures, selected in accordance with concrete mix designs commonly used in geotechnical engineering practice.

The conducted experiments were divided into two main groups: (i) tests aimed at determining the hydraulic properties, and (ii) investigations focusing on porosity and pore size distribution.

In the following sections, the measurement methodology applied during the investigations is presented, including a brief description of the measurement techniques, the boundary conditions applied, the storage conditions of the concrete samples, and the key characteristics of the tested specimens.

### 3.1 Concrete mixtures

During my experiments, the investigated concrete mixtures were classified into two groups based on the *constant* and *variable* parameters of the mix designs. When selecting the mix designs, I aimed to include mixtures that represent the widest possible range of concrete properties to ensure comprehensive coverage of material characteristics.

#### 3.1.1 First test group (M1–M18)

The first test group includes those concrete mixtures that were produced within the framework of Mónika Lombos’s diploma thesis (Lombos, 2016). When selecting the mix designs, my objective was to examine concrete types commonly used in geotechnical engineering practice. All mixtures in this group were produced using *CEM II A-S 42.5 R* type cement. In addition to variations in the water-to-cement ratio (0,40; 0,45; 0,50) and cement content (360 kg/m<sup>3</sup>; 400 kg/m<sup>3</sup>) some mixtures were modified with fiber reinforcement (steel or synthetic fibers) and/or admixtures designed to enhance watertightness (*Penetron ADMIX*). The maximum aggregate size was  $d_{\max}=16$  mm. The various combinations of mixing parameters resulted in a total of 18 different concrete compositions for the experiments, the main characteristics and variables of which are summarized in *Table 1*.

*Table 1 – Key variable parameters of the concrete mix designs in the first test group*

Mix.	Cement content [kg/m <sup>3</sup> ]	w/c [-]	Fiber reinforcement	Fiber content [kg/m <sup>3</sup> ]	Penetron [1 m%]	Label
M1	360	0.50	-	-	-	36-50
M2	360	0.45	-	-	-	36-45
M3	360	0.40	steel (Humix 50)	30	-	36-40-A
M4	400	0.50	steel (Humix 50)	30	-	40-50-A
M5	400	0.45	synthetic (Concrix)	3.5	-	40-45-M
M6	400	0.40	synthetic (Concrix)	3.5	-	40-40-M
M7	360	0.50	-	-	■	36-50-P
M8	360	0.45	-	-	■	36-45-P
M9	360	0.40	steel (Humix 50)	30	■	36-40-A-P
M10	400	0.50	steel (Humix 50)	30	■	40-50-A-P
M11	400	0.45	synthetic (Concrix)	3.5	■	40-45-M-P
M12	400	0.40	synthetic (Concrix)	3.5	■	40-40-M-P
M13	360	0.40	-	-	-	36-40
M14	360	0.40	-	-	■	36-40-P
M15	400	0.50	synthetic (Concrix)	3.5	-	40-50-M
M16	400	0.50	synthetic (Concrix)	3.5	■	40-50-M-P
M17	400	0.45	-	-	-	40-45
M18	400	0.45	-	-	■	40-45-P

### 3.1.2 Second test group (M19–M24)

The second test group includes the concrete grades investigated during my previous research activities. A total of six different concrete mixtures were available, incorporating two cement types (*CEM II A-S 42,5 N*; *CEM I 42,5 N-SR0*), three different cement contents (300 kg/m<sup>3</sup>; 360 kg/m<sup>3</sup>; 420 kg/m<sup>3</sup>), and three distinct water-to-cement ratios (0,42; 0,49; 0,59). The tested mixtures did not contain any fiber reinforcement or admixtures intended to improve watertightness. The maximum aggregate size was  $d_{\max}=8$  mm. The key variable parameters of the concrete mix designs in the second test group are summarized in Table 2.

Table 2 – Main variable parameters of the concrete mix designs in the second test group

Mix.	Cement content [kg/m <sup>3</sup> ]	Cement types	w/c [-]	Label
M19	300	CEM II A-S 42,5 N	0.59	30-59-II
M20	360	CEM II A-S 42,5 N	0.49	36-49-II
M21	420	CEM II A-S 42,5 N	0.42	42-42-II
M22	300	CEM I 42,5 N-SR0	0.59	30-59-I
M23	360	CEM I 42,5 N-SR0	0.49	36-49-I
M24	420	CEM I 42,5 N-SR0	0.42	42-42-I

### 3.1.3 Curing and storage conditions

The concrete specimens were consistently stored under combined curing and storage conditions. Following demoulding, the specimens were kept in lime-saturated water at a temperature of  $20 \pm 2$  °C until reaching an age of 7 days. Thereafter, until the commencement of the tests, the samples were stored at laboratory temperature ( $22 \pm 2$  °C, depending on the season) and in a laboratory environment ensuring a minimum relative humidity of 55%.

Given that the hydraulic tests to be performed could potentially extend over several weeks or even months, all measurements were initiated only after the specimens had reached an age of at least 100 days.

### 3.1.4 Concrete specimens

For both test groups, concrete cubes with dimensions of 150×150×150 mm were produced. In the case of the first test group, cylindrical samples with a nominal diameter of Ø50 mm were extracted from the cubes using diamond core drilling. Given that different testing methods require different sample heights, the core samples were subsequently cut into test specimens with heights ranging between 20 and 50 mm using a concrete cutting machine (*Figure 1*). For certain measurements (WP4C, MIP, SEM), it was necessary to prepare smaller samples with specific geometries and dimensions compared to the previously described specimens.



Figure 1 – Cylindrical samples

For the second test group, the cylindrical specimens were prepared by casting the concrete into copper rings with an internal diameter of  $\text{Ø}38$  mm and a nominal height of 20 mm. Compaction was performed using a vibrating table. After casting, the samples remained within the copper rings, which served as permanent moulds, and were tested in this condition.

## 3.2 Laboratory experiments

### 3.2.1 Determination of hydraulic properties

To determine the drying branch of the water retention curve, I applied three different measurement methods in order to cover the entire suction spectrum of the concrete mixtures. During the tests, the suction level was controlled, while the water content was determined by gravimetric measurements. Using sand and sand/kaolin boxes for the gravitational method, I covered the pF range between 0 and 2.7 (Stakman, et al., 1969; Várallyay, 1973). With the pressure membrane apparatus, the range between pF 3.0 and 4.2 was investigated (Klute, 1986; Imre, et al., 2008), while the desiccator-based method was applied to cover the suction range between pF 4.79 and 6.21 (Buzás, et al., 1993; Ng & Menzies, 2007). For each test, the required saturated state was achieved through capillary saturation. At each measurement point, mass measurements were performed weekly, biweekly, or monthly – depending on the rate of water loss – until mass equilibrium was reached, using a laboratory balance with a precision of 0.01 g. The experiments were carried out at the *Institute for Soil Science and Agricultural Chemistry of the Hungarian Academy of Sciences* and at the *Department of Engineering Geology and Geotechnics, Budapest University of Technology and Economics*.

To investigate the hysteresis between drying and wetting processes on the water retention curve of concrete, I used a WP4C device (METER Group Inc., 2024), which applies a chilled mirror dew point technique to determine the water potential of the samples. During testing, the water content of the specimens was gradually increased (wetting branch) and then decreased (drying branch), with 24-hour equilibration periods in sealed containers between each adjustment. Mass measurements were performed using a *Sartorius Entris 121i-1S* analytical balance with 0.1 mg precision. Experiments

were conducted in the *Soil Mechanics Laboratory at BUTE Department of Engineering Geology and Geotechnics*, following the *MSZ-08-0205:1978* and *ASTM D6836-16:2016* standards. At the end of each test series, samples were oven-dried at  $60\pm 5$  °C to avoid microstructural damage.

Saturated hydraulic conductivity was determined using a constant head permeability method with a *Wykeham Farrance*-type triaxial apparatus. Membrane-enclosed samples were placed in a water-filled cell, with back pressure applied via a compressor and cell pressure maintained at a higher level to prevent leakage between the sample and membrane. The hydraulic conductivity coefficient was calculated according to Darcy's law, with tests conducted under pressures ranging from 10 to 600 kPa, following *MSZE CEN ISO/TS 17892-11:2010*, in the *Soil Mechanics Laboratory at BUTE Department of Engineering Geology and Geotechnics*.

For validation purposes, I also performed standardized concrete watertightness tests according to *MSZ EN 12390-8:2009* on specimens cured under combined curing conditions. In these tests, a constant water pressure of 5 bar (500 kPa) was applied to 150 mm cubic specimens for 72 hours. After splitting the specimens, the maximum penetration depth was measured with millimeter accuracy, and water ingress patterns were documented to identify potential local anomalies. These tests were carried out at the *BUTE Department of Construction Materials and Technologies*, with evaluation based on the limit values defined in *MSZ 4798:2016/2M:2018*.

### 3.2.2 Investigation of the pore structure

To investigate the internal structure of the concrete, including cracks, voids, and pores, I used non-destructive X-ray computed tomography (CT) imaging, which is an effective tool for assessing durability-related properties and water transport behavior in concrete (Földes, 2006; Majorosné Lublói, et al., 2018; Csorba, et al., 2024). The CT scans were performed at the *Medical Imaging Clinic of the University of Pécs* using a *Siemens Somatom Perspective* CT scanner. The measurements were conducted with a voxel size of  $0.08\times 0.08\times 0.60$  mm, which allowed for the detection of pores larger than approximately 80  $\mu\text{m}$  in diameter. Three-dimensional image reconstruction was based on X-ray attenuation profiles (Kak & Slaney, 2001), and image processing was performed using the open-source software *ImageJ*.

For microstructural analysis at higher resolution, scanning electron microscopy (SEM) was applied. The SEM measurements were conducted at the *BUTE Department of Construction Materials and Technologies* using a *Thermo Fisher Phenom XL G2* desktop SEM. Prior to imaging, the samples were fractured to produce fresh surfaces and coated with a thin layer of gold to ensure electrical conductivity (Goldstein, et al., 2018). The SEM analysis allowed for the detailed characterization of the microstructure, including pore morphology and crack patterns.

To determine the pore size distribution and total porosity over a wide range (from a few nanometers to several hundred micrometers), mercury intrusion porosimetry (MIP) was performed. This method is based on the non-wetting behavior of mercury and the Washburn equation (Diamond, 2000). The MIP tests were carried out at the *SZIKKTI* laboratory using a *Quantachrome POREMASTER 60 GT* instrument, applying a contact angle of  $140^\circ$  and a mercury surface tension of  $0.484 \text{ N/m}$ . Before testing, the samples were oven-dried at  $60 \pm 5 \text{ }^\circ\text{C}$  to avoid thermally induced microstructural damage. Additionally, skeletal density was determined using an *Anton-Paar UltraPyc 5000* gas pycnometer. While MIP provides rapid and accurate determination of pore characteristics, its limitations include potential sample compression under high pressure and reduced sensitivity for larger pores (Lawrence, 1978; Thommes, et al., 2015).

### 3.3 Methodological overview

Figure 2 illustrates the experimental methods used for investigating the pore structure and hydraulic properties of concrete, along with the potential applications of the obtained data. A direct quantitative relationship exists between the pore size distribution and the water retention curve, allowing one function to be derived from the other (Rajkai, et al., 2015). Based on the water retention curve and the saturated hydraulic conductivity, the permeability function can be determined, which – along with the previously mentioned parameters – serves as a fundamental input for the numerical simulation of watertightness tests. The primary objective of the applied experimental and evaluation methods is to provide a more detailed and accurate description of water transport processes within concrete and to validate the experimental results through numerical modeling.

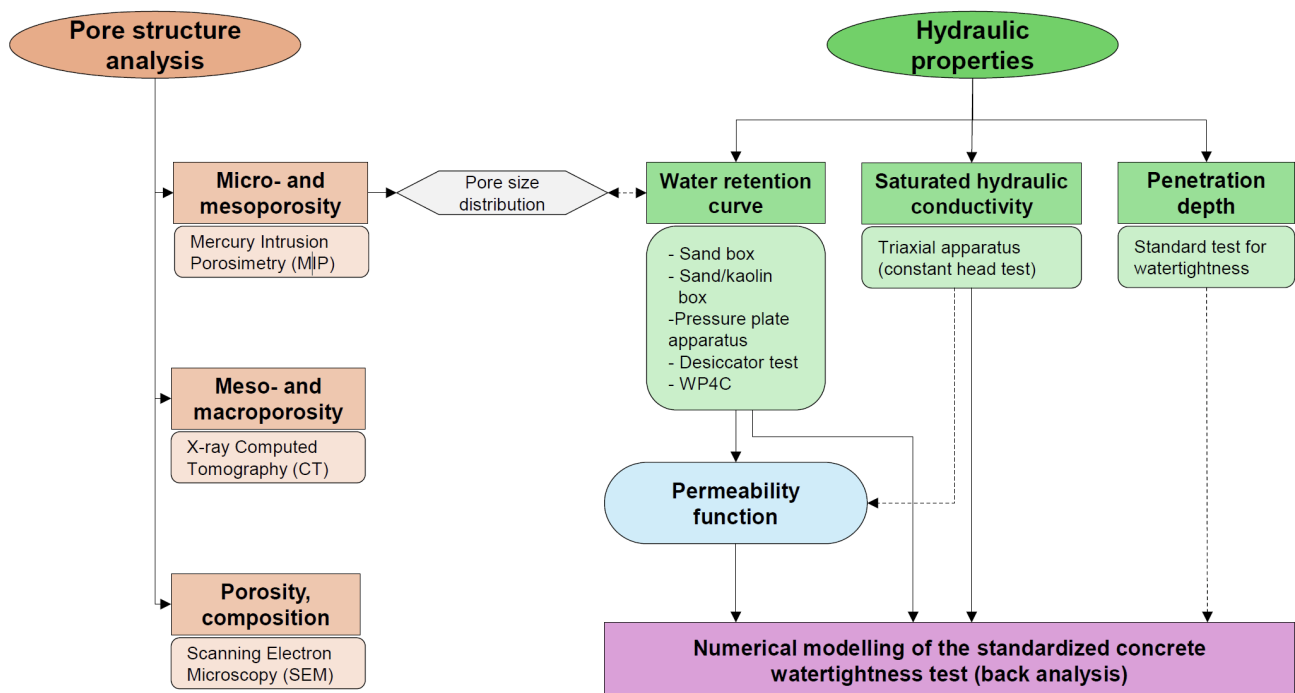


Figure 2 – Investigation and data processing workflow

The key data related to the test methods, testing conditions, and the examined concrete samples are summarized in *Table 3*.

*Table 3 – Experimental matrix*

Investigated properties	Measured parameter	Test equipment/ method	Relevant standard	Concrete mixes tested	Tested specimens			Storage conditions	Test temp.
					Number of Samples	Sample size (diameter, height, or edge length)	Age at testing [days]		
Hydraulic properties	Sand and sand/kaolin box (gravity method)		MSZ-08-0205:1978	M1–M18	36	Ø50±1 mm h=50±3 mm	ca. 150–300	21–23 °C	
				M1, M2, M5, M6, M7, M13, M15, M17	8	Ø50±1 mm h=24±4 mm	ca. 300–320	21–23 °C	
	Drying water retention curve (axis translation technique)	Desiccator test (vapor equilibrium technique)	ASTM D6836-16:2016	M1–M18	18	Ø50±1 mm h=30±1 mm	ca. 400–1000	21–23 °C	
				M1, M2, M13, M17	8	Ø35±1 mm h=5±1 mm	ca. 2000–2500	mixed storage (curing in water up to 7 days after demolding, then laboratory conditions until testing) RH≥55%, 22±2 °C	
Pore structure analysis	Hysteresis (wetting-drying)	WP4C device (chilled mirror dew point method)	ASTM D6836-16:2016	M1–M24	37	Ø50±1 mm Ø38 mm h=50±3 mm h=20±2 mm	ca. 150–300 ca. 100–150	22–24°C	
				M1–M24	72	150 × 150 × 150 mm	ca. 100–200	20–22°C	
	Saturated hydraulic conductivity	Triaxial apparatus (constant head test)	MSZE CEN ISO/TS 17892-11:2010	M1–M18	36	Ø50±1 mm h=50±3 mm	ca. 2100–2200	20–22°C	
				M1, M2, M13, M17	4	ca. 1 cm <sup>3</sup>	ca. 2100–2200	21–23 °C	
Maximum water penetration depth watertightness	Standard test for	X-ray Computed Tomography (CT)	EN 16016-2:2013	M1–M18	18	Ø0.5-1.0 cm	ca. 2100–2200	20–22 °C	
				M1–M18	18				

## 4 NUMERICAL MODELING OF WATER TRANSPORT

To evaluate the applicability and to provide a more detailed assessment of the material parameters determined during my research, I validated the measured saturated hydraulic conductivity values, the fitted wetting water retention curves, and the permeability functions derived from these curves through the numerical simulation of the standardized concrete water penetration test. For the verification of the modeling results, I used the average values of the maximum water penetration depths obtained from the water penetration tests. The numerical simulations were performed using the *Plaxis 2D Ultimate* finite element software.

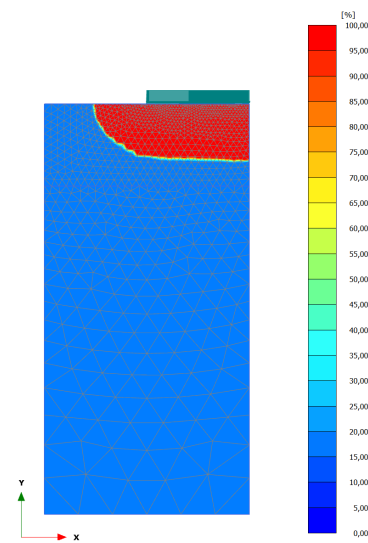


Figure 3 – Finite element model of the concrete specimen

To reduce computational demands during the model setup, I simplified the geometry of the concrete specimen by exploiting its symmetry, limiting the finite element model to half of the specimen (*Figure 3*). For mesh generation, I used two-dimensional triangular finite elements. To improve computational accuracy, the mesh density was further refined within a 30 mm thick zone expected to experience water penetration, applying a mesh coarseness factor of 0.2. The extent of mesh refinement was optimized through sensitivity analysis.

For seepage analysis, material parameters and state variables influencing water movement were required, including the saturated hydraulic conductivity, the initial suction value, and concrete-specific functions such as the water retention curve and the permeability function.

The sensitivity of the initial suction value was investigated by varying the starting relative humidity, based on the typical laboratory environmental conditions. The initial suction was set corresponding to relative humidity levels of 30%, 40%, 50%, 60%, and 70%.

As a boundary condition, a water pressure of 5 bar (500 kPa) was applied to the relevant surface of the model, in accordance with the test setup and symmetry considerations. A no-flow boundary condition was assigned along the symmetry axis. Water flow within the concrete was modeled as transient seepage, using predefined time intervals. Given that the standardized water penetration test lasts  $72 \pm 2$  hours, three timesteps (24 h, 48 h, and 72 h) were defined to track the entire process.

## 5 NEW SCIENTIFIC RESULTS

### STATEMENT (1)

Based on the measurements, I established a relationship between the maximum water penetration depth measured during the standardized concrete watertightness test and the saturated permeability coefficient for concrete specimens with a water-to-cement ratio ranging between 0.40 and 0.59, produced with blast furnace slag Portland cement or sulfate-resistant Portland cement, and aged at least 100 days. After demoulding, all specimens were stored for 7 days in lime-saturated water at a temperature of  $20 \pm 2$  °C, followed by storage under laboratory conditions ( $22 \pm 2$  °C, RH  $\geq$  55%) until the commencement of the tests. The resulting relationship can be expressed in the following form:

$$d_w = 1.74 \cdot 10^6 \sqrt{k} \quad (1)$$

where  $k$  is the saturated hydraulic conductivity [m/s], and  $d_w$  is the maximum water penetration depth [mm].

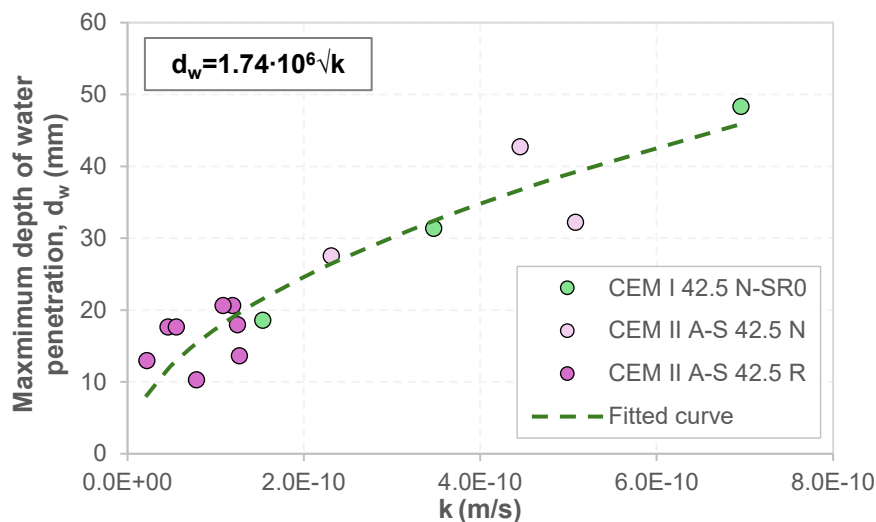


Figure 4 – Relationship between saturated permeability coefficient and maximum water penetration depth determined from the standard watertightness test

As an application of Equation (1), I determined the threshold values of saturated permeability coefficients corresponding to the watertightness classes defined by standards *MSZ 4798:2016* and *MSZ 4798:2016/2M:2018* for the investigated concrete grades (Table 4).

Table 4 – Watertightness classes with the corresponding threshold values of saturated permeability coefficients

Watertightness classes	Water penetration limit [mm]	Threshold value of permeability coefficient [m/s]
XV1(H)	50	$8.26 \cdot 10^{-10}$
XV2(H)	35	$4.05 \cdot 10^{-10}$
XV3(H)	20	$1.32 \cdot 10^{-10}$

Publications related to Statement (1): Pap et al. (2014); Pap et al. (2017)

## STATEMENT (2)

The measured drying water retention curves were fitted using both the van Genuchten (1980) model and the Fredlund & Xing (1994) model. Based on the sum of squared errors, the latter provided a better fit, indicating that it more accurately follows the water retention characteristics of concrete.

**Based on the experimental results, I found that for concretes produced with a water-to-cement ratio between 0.40 and 0.50 and using CEM II A-S 42.5 R type cement, the slope of the drying water retention curve in the transition zone decreases with increasing water-to-cement ratio. For the curves fitted with the Fredlund & Xing (1994) model, the  $n_f$  parameter – controlling the slope and associated with the pore size distribution – also decreases as the water-to-cement ratio increases.**

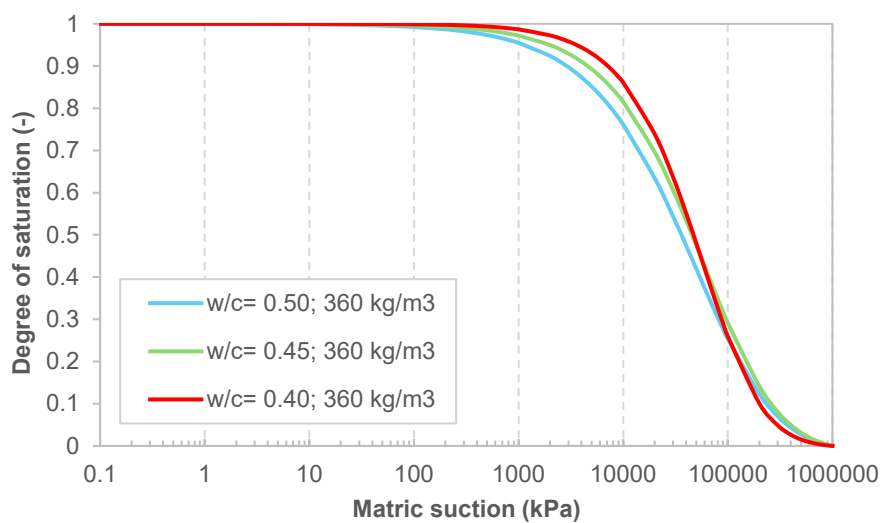


Figure 5 – Water retention curves of concrete mixtures without fiber reinforcement and Penetron admixture

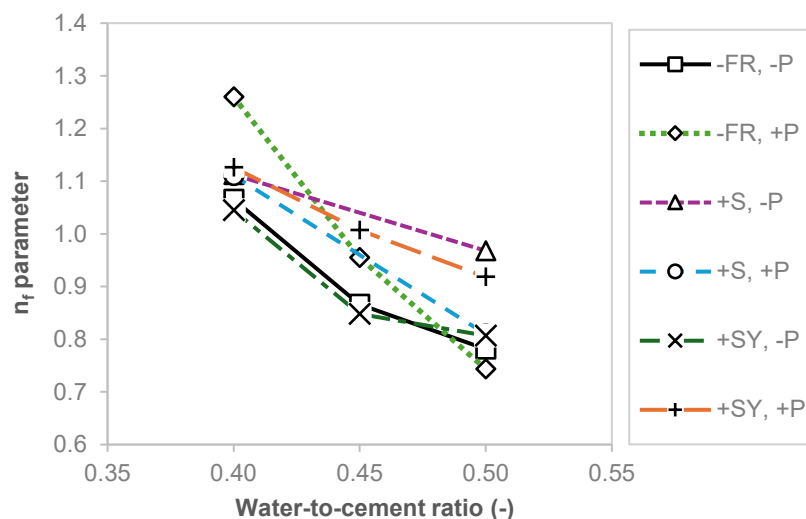


Figure 6 – Variation of the  $n_f$  parameter as a function of the water-to-cement ratio (FR: fiber reinforcement, S: steel, SY: synthetic, P: Penetron)

Publications related to Statement (2): Pap et al. (2018b); Pap et al. (2019b); Pap & Mahler (2025)

### STATEMENT (3)

The concept of lateral shift is frequently applied to estimate the wetting water retention curve from the drying branch. This method not only enables the approximation of the curve but also allows for the quantification of the hysteresis between the drying and wetting processes.

**Based on the measurements, I found that for concretes with a water-to-cement ratio between 0.40 and 0.50 and produced with CEM II A-S 42.5 R type cement, the hysteresis between the wetting and drying branches of the water retention curve – expressed in terms of the lateral shift value at the inflection point of the curves – varies between 40% and 90%. The wetting curves estimated by applying a lateral shift to the drying branch closely approximate the measured wetting branches within the suction range below 20,000 kPa. However, at higher suction values, discrepancies emerge that significantly affect the calculation of the wetting behavior of dry concrete.**

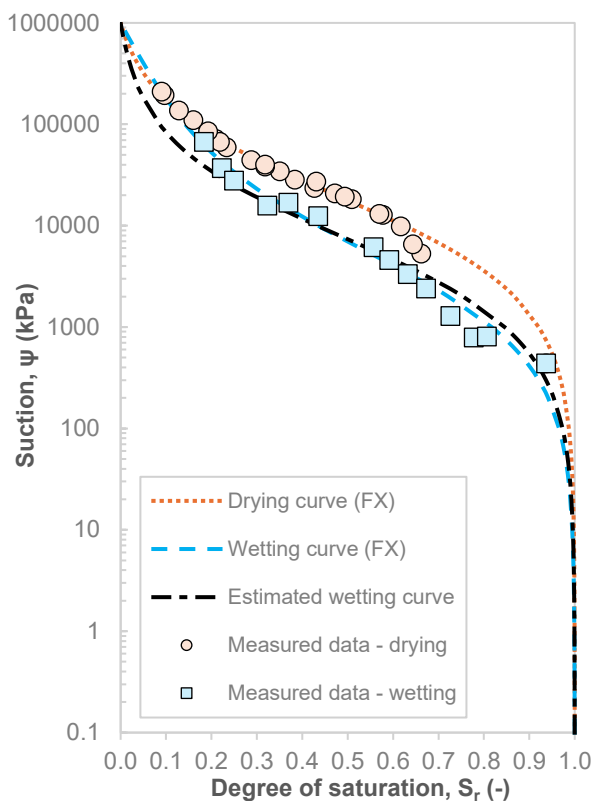


Figure 7 – Water retention curves of the M1 concrete mixture ( $w/c=0.50$ ;  $360 \text{ kg/m}^3$ ) fitted using the Fredlund & Xing (1994) model

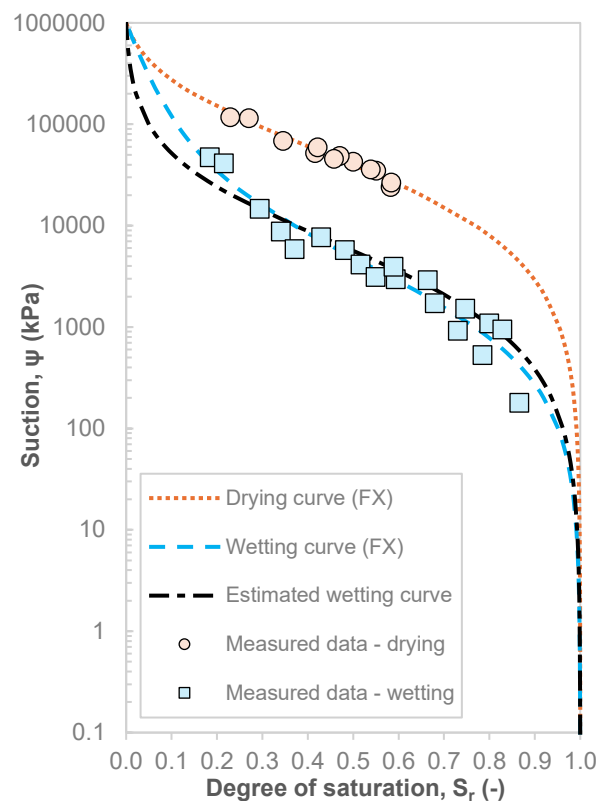


Figure 8 – Water retention curves of the M2 concrete mixture ( $w/c=0.45$ ;  $360 \text{ kg/m}^3$ ) fitted using the Fredlund & Xing (1994) model

## STATEMENT (4)

Through numerical analysis, I verified that for concrete, the calculation of the permeability function based on the measured and subsequently fitted water retention curves yields reliable results when applying the Fredlund et al. (1994) model.

**Based on the results of the numerical integration of the fitted water retention curves, I established that for concretes with a water-to-cement ratio between 0.40 and 0.50 and produced with CEM II A-S 42.5 R type cement, the relative permeability decreases with increasing water-to-cement ratio at a given suction level.**

The magnitude of this decrease can range from one to three orders of magnitude, depending on the specific concrete composition.

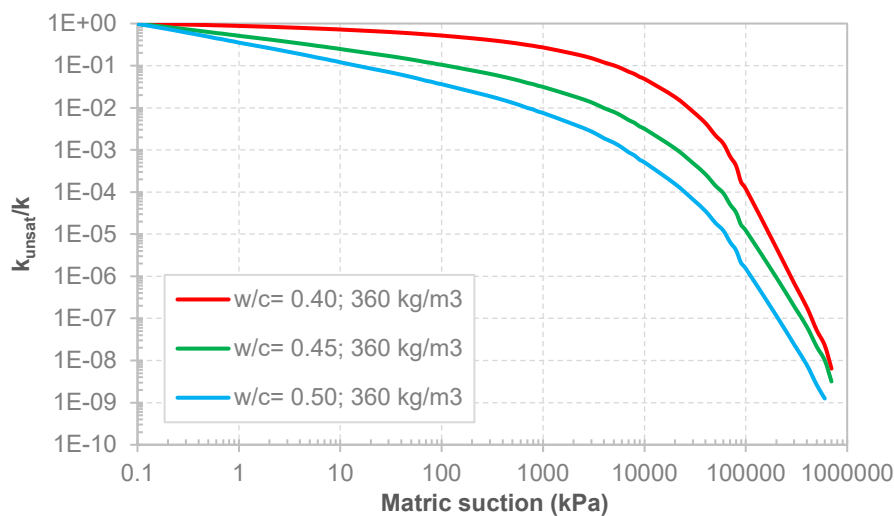


Figure 9 – Permeability functions of concrete mixtures without fiber reinforcement and Penetron admixture

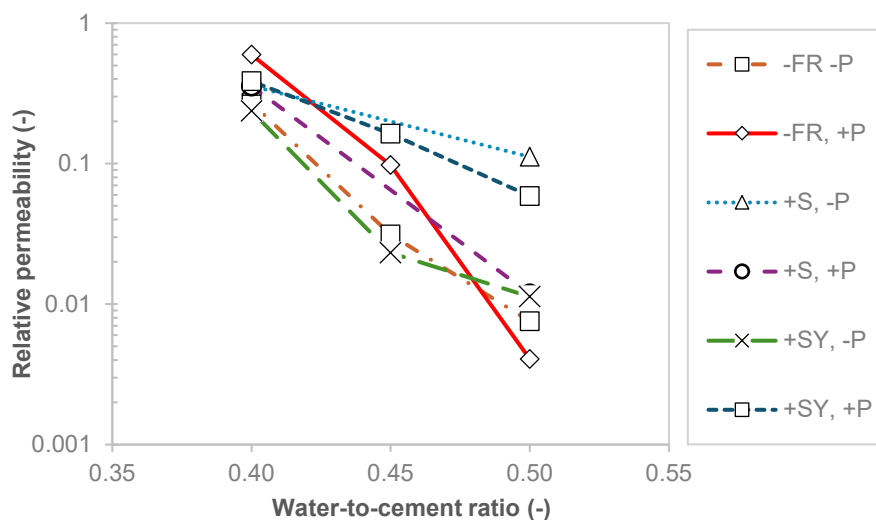


Figure 10 – Change in relative permeability with water-to-cement ratio at 1000 kPa suction  
 (FR: fiber reinforcement, S: steel, SY: synthetic, P: Penetron)

Publications related to Statement (4): Pap et al. (2018c); Pap et al. (2019b)

## STATEMENT (5)

Using numerical analysis in the *Plaxis 2D Ultimate* software, I modeled the standardized concrete watertightness test by applying the measured saturated hydraulic conductivity values, the wetting water retention curves fitted with the Fredlund & Xing (1994) model, and the permeability functions calculated using the model proposed by Fredlund et al. (1994). The simulations were conducted for five different initial suction levels (relative humidity conditions). The comparison between the simulation results and the laboratory watertightness test results confirmed that the permeability functions derived from the water retention curves can be reliably used for modeling water transport in concrete.

**Based on the results of the numerical simulations performed using parameters determined from the experimental measurements, I concluded that an increase in the initial relative humidity – within the range of 30% to 70% – results in an increase in the maximum water penetration depth. This finding indicates that both the storage conditions of the concrete specimens and the relative humidity during testing may influence the maximum water penetration depth.**

A 10% increase in relative humidity may result in a 19–49% increase in the maximum water penetration depth, depending on the concrete type.

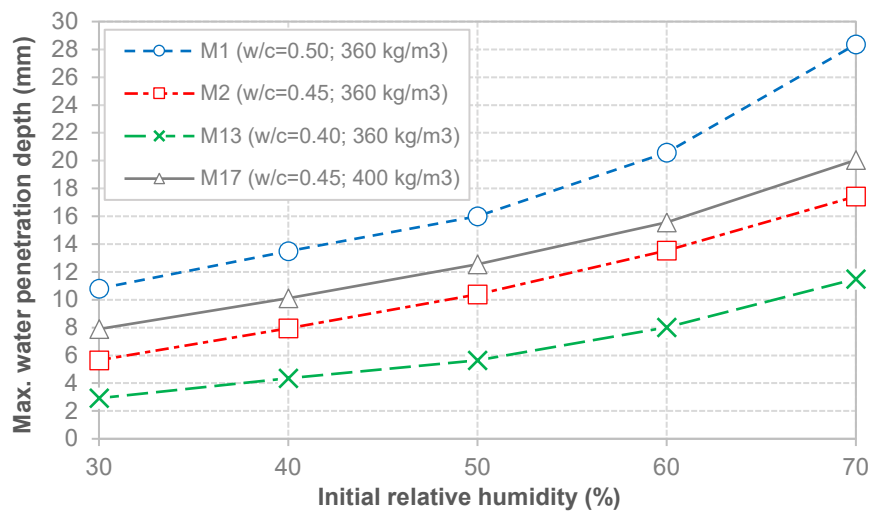


Figure 11 – Maximum water penetration depth as a function of the initial relative humidity

Based on my investigations, it would be advisable to develop more precise guidelines regarding the following aspects:

- the required time frame within which the test should be conducted after removing the specimens from water storage, and
- the appropriate temperature and relative humidity conditions for both storage and testing in the case of specimens subjected to combined curing.

*Publications related to Statement (5): Pap et al. (2018a); Pap et al. (2018c); Pap et al. (2024); Pap & Mahler (2025)*

## **6 APPLICATION OF THE RESULTS**

During the laboratory investigations, I determined the key material parameters required for the numerical modeling of water transport processes in concrete and validated their applicability through computer-based simulations. The research contributes to improving the accuracy of laboratory measurements and enables the reliable modeling of water transport phenomena in concrete. The applied testing and evaluation methodology revealed the interrelationships between concrete composition and its water retention, watertightness, and permeability characteristics.

The results provide a basis for simulating water movement in radioactive waste repositories, ensuring the exclusion of both external and internal water transport over the entire service life. Similarly, the findings support the calculation of water movement in underground concrete structures, such as tunnels and diaphragm walls. Furthermore, this research establishes a foundation for the optimization of concrete mix designs regarding watertightness and water transport properties, thereby contributing to the design of durable, sustainable, and cost-effective concrete structures.

## **7 FUTURE RESEARCH**

The relationships identified during this research may serve as a basis for further investigations. Particular attention should be given to the detailed analysis of the hysteresis observed in the water retention curve, which could enhance the understanding of the differences between wetting and drying processes. Another potential research direction is the examination of the relationship between pore size distribution and water retention curves. This could contribute to a more accurate characterization of the pore structure and water retention capacity of concrete, as well as enable the estimation of water retention curves based on pore structure data.

In addition, it is recommended to explore the correlations between saturated hydraulic conductivity, concrete composition and porosity, hydraulic conductivity anisotropy, and the shape of water penetration fronts. The combined application of porosity measurement methods – particularly CT and MIP techniques – appears promising for determining the complete pore size distribution, thereby refining water retention characteristics and improving the parameterization required for water transport modeling.

Based on the numerical modeling results, an increase in the initial relative humidity leads to greater water penetration depths. The quantitative interpretation of this effect requires further laboratory testing under different initial humidity conditions. Such studies could support a more accurate and comprehensive understanding of water transport and water tightness in concrete, and may contribute to the further development of standardized testing methods.

## 8 AUTHOR'S PUBLICATIONS RELATED TO THE TOPIC

- Pap, M., Mahler, A. & Nehme, S. G., 2014. Betonok áteresztőképességi együtthatójának meghatározása. In: Z. Tompai, A. Mahler, A. Takács & G. Varga, ed. *Geotechnika 2014 Konferencia*. Budapest: Konferencia Iroda Bt, p. 23.
- Pap, M., Mahler, A. & Nehme, S. G., 2015. A betonokban történő vízmozgás vizsgálata és modellezése. *VASBETONÉPÍTÉS*, 17(3), pp. 56-63.
- Pap, M., Mahler, A. & Nehme, S. G., 2016. Szabványos beton vízzáróság vizsgálat numerikus modellezése. In: G. Köllő, ed. *XX. Nemzetközi Építéstudományi Konferencia: ÉPKO 2016 - 20th International conference on civil engineering and architecture*. Cluj-Napoca, Romania: Erdélyi Magyar Műszaki Tudományos Társaság (EMT), pp. 205-208.
- Pap, M., Mahler, A. & Nehme, S. G., 2017. Betonszerkezetek vízzárósága és áteresztőképessége. *MŰSZAKI ELLENŐR*, 6(5), pp. 35-38.
- Pap, M., Mahler, A. & Nehme, S. G., 2018a. Finite element modelling of seepage in concrete. In: *XVI DECGE 2018 Proceedings of the 16th Danube - European Conference on Geotechnical Engineering*. Berlin, Germany: Ernst und Sohn, pp. 737-742.
- Pap, M., Mahler, A. & Nehme, S. G., 2018b. Measurement of water retention curve for different concrete mixtures. In: *The 7th International Conference on Unsaturated Soils*. Hongkong: UNSAT2018, pp. 363-367.
- Pap, M., Mahler, A. & Nehme, S. G., 2018c. Analysis and Finite Element Modelling of Water Flow in Concrete. *Periodica Polytechnica Civil Engineering*, 62(4), pp. 1052-1059.
- Pap, M., Mahler, A. & Nehme, S. G., 2019a. Betonok telítetlen áteresztőképesség-függvényének meghatározása. In: T. Huszák, ed. *5. Kézdi Konferencia*. Pécs, Hungary: Magyar Geotechnikai Egyesület, pp. 307-316.
- Pap, M., Mahler, A. & Nehme, S. G., 2019b. Estimation of permeability function for concrete. In: H. Sigursteinsson, S. Erlingsson & B. Bessason, ed. *XVII European Conference on Soil Mechanics and Geotechnical Engineering - Reykjavík, Iceland: 1-6 of September 2019: Geotechnical Engineering, foundation of the future: Conference proceedings*. Reykjavík, Iceland: Icelandic Geotechnical Society, p. 7.
- Pap, M., Mahler, A., 2019c. Comparison of different empirical correlations to estimate permeability coefficient of Quaternary Danube soils. *Periodica Polytechnica Civil Engineering*, 63(1), pp. 25-29.
- Pap, M., Mahler, A. & Nehme, S. G., 2020. Laboratory testing of seepage in concrete. *E3S Web of Conferences*, 195(-), p. 03030.

- Pap, M., Mahler, A. & Nehme, S. G., 2022. Laboratory testing of water flow in building materials. In: M. Rahman & M. Jaksa, ed. *Proceedings of the 20th International Conference on Soil Mechanics and Geotechnical Engineering*. Sydney, Australia: Australian Geomechanics Society, pp. 191-195.
- Pap, M., Mahler, A., Illés, Z. & Nehme, S. G., 2024. Laboratory testing and numerical modelling of seepage in building materials. In: N. Guerra, et al. ed. *Geotechnical Engineering Challenges to Meet Current and Emerging Needs of Society: Proceedings of the XVIII ECSMGE 2024*. Lisbon: CRC Press, pp. 3206-3211.
- Pap, M. & Mahler, A., 2025. Víztartási görbe hiszterézisének vizsgálata különböző betonok esetén. In: Á. Török, B. Vásárhelyi & P. Görög, ed. *Mérnökgeológia-Kőzetmechanika 2025*. Budapest: BME Geotechnika és Mérnökgeológia Tanszék, pp. -. (megjelenés alatt)

## 9 REFERENCED STANDARDS

ASTM D6836-16:2016	Standard Test Methods for Determination of the Soil Water Characteristic Curve for Desorption Using a Hanging Column, Pressure Extractor, Chilled Mirror Hygrometer, or Centrifuge
MSZ 4798:2016	Concrete – Technical requirements, properties, production, conformity and the conditions for the application of EN 206 in Hungary
MSZ 4798:2016/2M:2018	Concrete – Technical requirements, properties, production, conformity and the conditions for the application of EN 206 in Hungary (Amendment to MSZ 4798:2016)
MSZ EN 12390-8:2009	Testing hardened concrete – Part 8: Depth of penetration of water under pressure
MSZ-08-0205:1978	Testing the physical and water management properties of soils
MSZE CEN ISO/TS 17892-11:2010	Geotechnical investigation and testing – Laboratory testing of soil – Part 11: Determination of permeability by constant and falling head

## 10 REFERENCES

- Buzás, I. et al., 1993. *Talaj- és agrokémiai vizsgálati módszerkönyv I.*. Budapest: INDA 4231 Kiadó.
- Carme, M. C. & Saaltink, M. W., 2016. Water, vapour and heat transport in concrete cells for storing radioactive waste. *Advances in Water Resources*, 94(-), pp. 120-130.
- Csorba, K. et al., 2024. Monitoring of historical structural materials with computed tomography. *Structural Concrete*.
- Darcy, H., 1856. *Les fontaines publiques de la ville de Dijon*. Dalmont, Paris: s.n.
- Diamond, S., 2000. Mercury porosimetry: An inappropriate method for the measurement of pore size distributions in cement-based materials. *Cement and Concrete Research*, 30(10), pp. 1517-1525.

- Fleming, I. R., Andree, M. G. & Fourmont, S., 2023. Efficacy of Nonwoven Based Geosynthetic Drainage Product for Pore Pressure Reduction in Moderately Fine Soils or Tailings. *Geosynthetics Conference*, 1(-), pp. 277-287.
- Földes, T., 2006. Röntgen computer tomográf (CT) mérések alkalmazási lehetőségei a kőzetvizsgálatokban. *Mérnökgeológia-Kőzetmechanika*.
- Fredlund, D. G., Rahardjo, H. & Fredlund, M. D., 2012. *Unsaturated Soil Mechanics in Engineering Practice*. Hoboken, New Jersey: John Wiley & Sons, Inc..
- Fredlund, D. G. & Xing, A., 1994. Equations for the soil-water characteristic curve. *Canadian Geotechnical Journal*, 31(4), pp. 521-532.
- Fredlund, D. G., Xing, A. & Huang, S., 1994. Predicting the permeability function for unsaturated soils using the soil-water characteristic curve. *Canadian Geotechnical Journal*, 31(4), pp. 533-546.
- Goldstein, J. I. et al., 2018. *Scanning Electron Microscopy and X-ray Microanalysis*. Boston: Springer.
- Imre, E. et al., 2008. A homokfrakciók és homokkeverékek víztartási görbéje közötti kapcsolat. *Hidrológiai Közlöny*, 88(5), pp. 52-56.
- Kak, A. C. & Slaney, M., 2001. *Principles of Computerized Tomographic Imaging*. -: IEEE Press.
- Klute, A., 1986. Water Retention: Laboratory Methods. In: *Methods of Soil Analysis: Part 1*. Madison, WI, USA: Soil Science Society of America, American Society of Agronomy, pp. 635-662.
- Lawrence, G. P., 1978. Stability of soil pores during mercury intrusion porosimetry. *Journal of Soil Science*, 29(3), pp. 299-304.
- Leech, C., Lockington, D. & Dux, P., 2003. Unsaturated diffusivity functions for concrete derived from NMR images. *Materials and Structures*, 36(-), pp. 413-418.
- Leech, C. A., 2003. *Water Movement in Unsaturated Concrete: Theory, Experiments, Models*. Queensland: Department of Civil Engineering The University of Queensland.
- Liu, Z., Zhang, P., Bao, J. & Hu, Y., 2020. Numerical Simulation of Water Transport in Unsaturated Recycled Aggregate Concrete. *Frontiers in Materials*, 7(-), pp. -.
- Lombos, M., 2016. *Penetron hatása a vízzáróságra (BSc diplomamunka)*. Budapest: Budapesti Műszaki és Gazdaságtudományi Egyetem, Építőmérnöki Kar.
- Major, J. & Wittmann, F. H., 2011. Zwei-Phasen Strömung in Zement gebundenen Werkstoffen. *Restoration of Buildings and Monuments*, 17(2), pp. 111-116.
- Major, J., Wittmann, F. H. & Sadouki, H., 2010. Drying and Hygral Diffusion Coefficient of Concrete. *Restoration of Buildings and Monuments*, 16(1), pp. 39-46.
- Majorosné Lublóy, É. E. et al., 2018. CT alkalmazási lehetőségei az építőanyagok vizsgálatánál. *Vasbetonépítés*, 20(4), pp. 89-93.
- Ma, S., Yao, Y., Bao, P. & Guo, C., 2023. Effects of moisture content on strength and compression properties of foundation soils of cultural relics in areas flooded by the Yellow River. *Frontiers in Materials*, 10(-), pp. -.

- METER Group Inc., 2024. *WP4C Dew Point PotentiaMeter Operator's Manual*. Pullman, USA: METER Group Inc.
- Mualem, Y., 1976. A new model for predicting the hydraulic conductivity of unsaturated porous media. *Water Resources Research*, 12(3), pp. 513-522.
- Ng, C. W. W. & Menzies, B., 2007. *Advanced Unsaturated Soil Mechanics and Engineering*. London, and New York: Taylor and Francis.
- Pap, M., Mahler, A. & Nehme, S. G., 2018. Analysis and Finite Element Modelling of Water Flow in Concrete. *Periodica Polytechnica Civil Engineering*, 62(4), pp. 1052-1059.
- Park, K. & Fleming, I., 2006. Evaluation of a geosynthetic capillary barrier. *Geotextiles and Geomembranes*, 24(1), pp. 64-71.
- Pezowicz, P. & Choma-Moryl, K., 2015. Moisture Content Impact on Mechanical Properties of Selected Cohesive Soils from the Wielkopolskie Voivodeship Southern Part. *Studia Geotechnica et Mechanica*, 37(4), pp. 37-46.
- Rajkai, K. et al., 2015. Particle-size and organic matter effects on structure and water retention of soils. *Biologia*, 70(11), pp. 1456-1461.
- Renken, L., Oeser, M., Milatz, M. & Grabe, J., 2016. Measurement of hydraulic properties of unsaturated permeable polyurethane bound asphalt materials. In: *Unsaturated Soil Mechanics - from Theory to Practice: Proceedings of the 6th Asia Pacific Conference on Unsaturated Soils*. Guilin, China: CRC Press, pp. 407-412.
- Stakman, W. P., Valk, G. A. & van der Harst, G. G., 1969. *Determination of soil moisture retention curves I.* Wageningen: Instituut voor Cultuurtechniek en Waterhuishouding.
- Thommes, M. et al., 2015. Physisorption of gases, with special reference to the evaluation of surface area and pore size distribution (IUPAC Technical Report). *Pure and Applied Chemistry*, 87(9-10), pp. 1051-1069.
- Törzs, T. et al., 2019. Hydraulic properties of polyurethane-bound permeable pavement materials considering unsaturated flow. *Construction and Building Materials*, 212(-), pp. 422-430.
- van Genuchten, M. T., 1980. A Closed-form Equation for Predicting the Hydraulic Conductivity of Unsaturated Soils. *Soil Science Society of America Journal*, 44(5), pp. 892-898.
- Várallyay, G., 1973. A talajok nedvességpotenciálja és új berendezés annak meghatározására az alacsony (atmoszféra alatti) tenziótartományban. *Agrokémia és Talajtan*, Volume 22, pp. 1-22.
- Vásárhelyi, B. & Davarpanah, M., 2018. Influence of Water Content on the Mechanical Parameters of the Intact Rock and Rock Mass. *Periodica Polytechnica Civil Engineering*, 62(4), pp. 1060-1066.
- Vilasboas, J. M. L., Machado, S. L. & Pinto, S. A., 2016. Filter paper method to determine the water retention curves for mortar and cement samples. *Revista IBRACON de Estruturas e Materiais*, 9(4), pp. 525-533.
- Washburn, E. W., 1921. The Dynamics of Capillary Flow. *Physical Review*, 17(3), pp. 273-283.
- Zhang, Q. et al., 2023. Study on the Effects of Different Water Content Rates on the Strength and Brittle Plasticity of Limestone. *Applied Sciences*, 13(8), p. 4685.